

Notice: This manuscript has been authored by UT-Battelle, LLC, under Contract No. DE-AC0500OR22725 with the U.S. Department of Energy. The United States Government retains and the publisher, by accepting the article for publication, acknowledges that the United States Government retains a non-exclusive, paid up, irrevocable, world-wide license to publish or reproduce the published form of this manuscript, or allow others to do so, for the United States Government purposes. The Department of Energy will provide public access to these results of federally sponsored research in accordance with the DOE Public Access Plan (<http://energy.gov/downloads/doe-public-access-plan>).

## MESOSCOPIC THEORY OF DEFECT ORDERING-DISORDERING TRANSITIONS IN THIN OXIDE FILMS

Anna N. Morozovska<sup>1\*</sup>, Eugene A. Eliseev<sup>2</sup>, Maya D. Glinchuk<sup>2</sup>, Rama Vasudevan<sup>3</sup>, Maxim V. Silibin<sup>4a,b</sup>, Yuri A. Genenko<sup>5†</sup> and Sergei V. Kalinin<sup>3 ‡</sup>

<sup>1</sup>*Institute of Physics, National Academy of Sciences of Ukraine,  
46, pr. Nauky, 03028 Kyiv, Ukraine*

<sup>2</sup>*Institute for Problems of Materials Science, National Academy of Sciences of Ukraine,  
Krjijanovskogo 3, 03142 Kyiv, Ukraine*

<sup>3</sup>*The Center for Nanophase Materials Sciences, Oak Ridge National Laboratory,  
Oak Ridge, TN 37922*

<sup>4a</sup>*National Research University of Electronic Technology "MIET", 124498 Moscow, Russia*

<sup>4b</sup>*Institute for Bionic Technologies and Engineering, I.M. Sechenov First Moscow State Medical  
16 University, Moscow 119991, Russia*

<sup>5</sup>*Institute of Materials Science, Technische Universität Darmstadt, Otto-Berndt-Str.3,  
Darmstadt, Germany*

### Abstract

Ordering of mobile defects in functional materials can give rise to fundamentally new phases possessing ferroic and multiferroic functionalities. Here we develop the Landau theory for strain induced ordering of defects (e.g. oxygen vacancies) in thin oxide films, considering both the ordering and wavelength of possible instabilities. Using derived analytical expressions for the energies of various defect-ordered states, we calculated and analyzed phase diagrams dependence on the film-substrate mismatch strain, concentration of defects, and Vegard

---

\* Corresponding author: [anna.n.morozovska@gmail.com](mailto:anna.n.morozovska@gmail.com)

† Corresponding author: [genenko@mm.tu-darmstadt.de](mailto:genenko@mm.tu-darmstadt.de)

‡ Corresponding author: [sergei2@ornl.gov](mailto:sergei2@ornl.gov)

coefficients. Obtained results open possibilities to create and control superstructures of ordered defects in thin oxide films by selecting the appropriate substrate and defect concentration.

## I. INTRODUCTION

Ferroelectric and multiferroic materials are the object of much fascination in physics community, both due to the multitude of possible applications and broad spectrum of fundamental physical phenomena they exhibit. Applications such as ferroelectric memories, field effect transistors, and domain wall conductance have riveted attention of scientific community in the last two decades [1, 2, 3]. Similarly, the nature of ferroelectric transitions, ferroelectricity in disordered systems, etc. remain a subject of active research since the discovery of ferroelectricity in late 1920ies [4]. Topological defects in ferroelectric materials and coupling between the ferroelectric and semiconductor subsystems are actively explored in the context of surface and domain wall conductance [5, 6, 7, 8].

From the gamut of possible behaviors, in the last decade progressively more attention is focused on multiferroic materials, i.e. systems possessing two or more order parameters [9, 10, 11, 12]. These functionalities significantly broaden the spectrum of possible applications, including oxide nanoelectronics, sensors and actuators, and IoT devices [13, 14, 15, 16]. Furthermore, in multiferroic materials fundamentally new properties can emerge at the topological defects [17]. Examples of the former include the emergence of suppressed order parameter and associated topological defects at the domain walls, surfaces and interfaces, domain wall and vortex core conduction, incipient ferroelectricity and magnetism, and many others [8, 18, 19].

The vast majority of the research in the field explored the coupling between the primary physical order parameters including magnetization, polarization, and ferroelasticity [8,18]. However, it is well known that chemical degrees of freedom can strongly affect the ferroelectric behavior [20]. A number of groups explored the phenomena such as vacancy segregation at the domain walls and grain boundaries [21, 22, 23, 24, 25], or changes in surface reactivity in response to polarization [26, 27]. However, most of these works explore the responses of chemical subsystems to the polarization. Relatively small effort was dedicated to the exploration of chemical effects on polarization [28, 29, 30], typically the surface electrochemistry including chemically-induced switching [31, 32, 33, 34] and emergence of ferroionic phases [35, 36, 37].

This direction has acquired particular prominence with the advent of the hybrid perovskites where chemical subsystem is strongly coupled to the environment and electrode phenomena (see e.g. review [38] and refs therein). However, the volume of research in this field is limited.

Here, we develop an initial framework for mesoscopic theory of defect ordering-disordering transitions in thin oxide films. We explore whether chemically induced changes in Vegard volume can be used to trigger and control ferroic orderings in thin strained films, and what the properties of such systems.

## II. TWO SUB-LATTICES MODEL OF POINT DEFECTS ORDERING

Here we consider the case of a thin oxide film on a substrate, taking into account the misfit strain [39], while neglecting the appearance of misfit dislocations. This assumption is generally valid for the films with a thickness smaller than a critical value ( $\sim 10\text{-}50$  nm) corresponding to dislocation nucleation [40]. The geometry of the problem is shown in **Fig. 1**. For high enough concentration of neutral/charged vacancies, the vacancy-ordered state can emerge [41] leading to the appearance of an elastic/electric dipole sublattice.

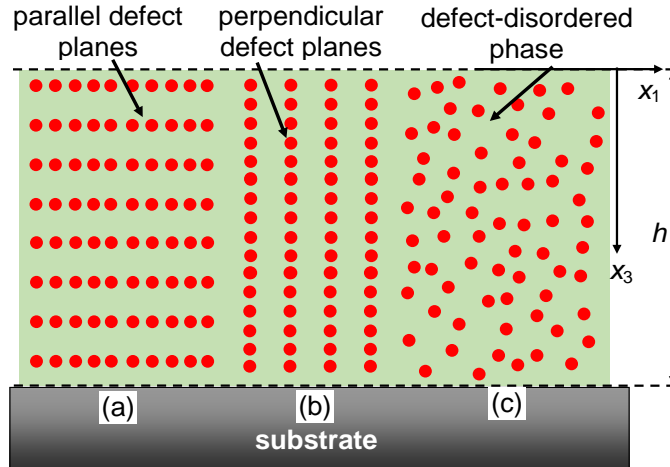


**FIGURE 1.** Point defect ordering in ultra-thin oxide film of thickness  $h$  placed on a rigid substrate. One can distinguish parallel (**a**, the left side) and perpendicular (**b**, the central part) orientations of the defect sub-lattices planes from the state with randomly distributed defects (**c**, the right side).

To describe the phase ordering process, we introduce a dimensionless order parameter  $\eta$ , related to the degree of ordering of point defects (oxygen or cation vacancies, or impurity atoms)

and given here by a disbalance of occupations of two sub-lattices. The scalar order parameter  $\eta$  is introduced as normalized occupation degree of the sub-lattices,  $0 \leq |\eta| \leq 1$ . For given  $\eta$ , the relative occupation numbers for the two sub-lattices are  $\delta n_a = c(1-\eta)/(2c_0)$  and  $\delta n_b = c(1+\eta)/(2c_0)$ . The total occupation of two sub-lattices is constant,  $\delta n_a + \delta n_b = c/c_0$ . Here  $c$  is the concentration of defects related with the non-stoichiometry degree  $\delta$ ;  $c_0$  is a characteristic value that usually coincides with the solubility limit, meaning that the defect atoms do not affect essentially the host lattice force matrix at  $c < c_0$ . Note that  $c_0 < N_a$ , where  $N_a$  is the stoichiometric concentration of host atoms.

In the particular case of oxygen vacancies,  $c$  depends on the oxygen pressure  $p$  via the defect equilibria and for certain cases  $\frac{c}{c_0} \sim \delta \sim \ln\left(\frac{p_0 + A(T)p}{p_0}\right)$  (e.g. see Fig. 3 in Ref. [42]).

Following the theory by Khachatryan [43], we assume that concentration  $c$  is coordinate-independent [44]. Values  $\eta = \pm 1$  correspond to the complete ordering of defects in either sub-lattice “b” or “a”, while  $\eta = 0$  corresponds to the complete disorder (with equal filling of two sub-lattices).

The defect sub-lattices ordering direction can be different with respect to the film surfaces. Below we will distinguish parallel [see the left side **(a)** in **Fig. 1**] and perpendicular [see the central part **(b)** in **Fig. 1**] orientations of defect sub-lattices.

The  $\eta$ -dependent free energy of a thin film is

$$F = \frac{\alpha_s}{2} \int_{S_F} [\eta^2(x_1, x_2, 0) + \eta^2(x_1, x_2, h)] dx_1 dx_2 + \int_{V_F} f dx_1 dx_2 dx_3, \quad (1a)$$

where  $h$  is the film thickness, and the first term is the surface/interface energy that is not negative under the condition  $\alpha_s \geq 0$ . Hereinafter we will consider the case  $\alpha_s = 0$ , corresponding to the so-called natural boundary conditions.

The bulk density,  $f$ , of the Helmholtz free energy expansion on the order parameter has the form:

$$f = \frac{\alpha}{2} c^2 \eta^2 + c \frac{k_B T}{2} [(1-\eta)\ln(1-\eta) + (1+\eta)\ln(1+\eta)] \\ + \frac{g_{ij} c^2}{2} \frac{\partial \eta}{\partial x_i} \frac{\partial \eta}{\partial x_j} + \frac{w_{ijkl} c^2}{2} \frac{\partial^2 \eta}{\partial x_i \partial x_j} \frac{\partial^2 \eta}{\partial x_k \partial x_l} + q[\eta, \sigma_{ij}] \quad (1b)$$

The first term in Eq. (1b) determines the interaction between the defects. Hereinafter we will consider both cases  $\alpha < 0$  and  $\alpha > 0$ . For the former, defects may order spontaneously in a bulk material, while in the latter case the ordering in bulk is unfavorable, but can be induced by external factors (such as misfit strain).

The second term is the entropy of the system. The third and the fourth terms are the series expansion of generalized gradient-correlation energy on the derivatives  $\partial\eta/\partial x_i$  of the order parameter. Below we consider the tensors  $g_{ij}$  and  $w_{ijkl}$  in isotropic approximation,  $g_{ij} = g\delta_{ij}$  and  $w_{ijkl} = w\delta_{ij}\delta_{kl}$ , and explore the case of  $w > 0$ . This choice is because we study the case of the defects ordering for positive correlation energy.

Note that very often the higher gradient term is neglected ( $w = 0$ ). Rigorously it is justified only if  $g > 0$ , assuming that its renormalization by the strain gradient energy is either positive or too small to change the positive sign of resulting effective gradient coefficient. Below we will show that  $w$ -term is mandatory to determine the threshold for emergence of the order parameter spatial modulation.

The elastic energy  $q[\eta, \sigma_{ij}]$  includes the coupling between the order parameter and the stresses  $\sigma_{ij}$ . Following the theoretical formalism of Vegard strains proposed by Freedman [45] and using the strain energy of Levanyuk et al. [46], the coupling term between the order parameter and the stresses could be also expanded as a series on the order parameter:

$$q[\eta, \sigma_{ij}] = -\frac{s_{ijkl}}{2}\sigma_{ij}\sigma_{kl} + u_{ij}\sigma_{kl} - V_{ij}\sigma_{ij}c - \frac{B_{ijmm}}{2}\sigma_{ij}c^2 \frac{\partial\eta}{\partial x_m} \frac{\partial\eta}{\partial x_n}. \quad (1c)$$

Here  $s_{ijkl}$  is the elastic compliances tensor, and  $u_{ij}$  is the tensor of elastic strains. To describe the mixed mechanical state of the epitaxial binary oxide film on the substrate, we perform the Legendre transform by adding the term  $u_{kl}\sigma_{kl}$ . The third term in Eq. (1c) is the chemical expansion due to the appearance of elastic defects, characterized by the Vegard strain tensor  $V_{ij}$ . The Vegard contribution is  $\eta$ -independent, since  $\delta n_a + \delta n_b = c/c_0$ . Symmetry of  $V_{ij}$  is determined by the local site symmetry of defect with respect to the lattice, which could be different from the lattice symmetry (see e.g. Ref. [45] considering different vacancies in SrTiO<sub>3</sub>).

It will be shown that the last term in Eq. (1c) plays a central role in the mechanism of defect ordering. It is a gradient-type striction due to the defect ordering that is characterized by a

fourth rank tensor  $B_{ijkl}$ . Note that the term linear in  $\eta$  is excluded from Eq. (1c) since both sublattices are equivalent with respect to the corresponding translation.

In the continuous media approximation, the thermodynamically stable state of the film can be derived from the variation of the free energy (1) on  $\eta$  and  $\sigma_{ij}$ , leading to Euler-Lagrange differential equations:

$$\alpha c^2 \eta + c k_B T \operatorname{arctanh}(\eta) + c^2 B_{ijmn} \frac{\partial \sigma_{ij}}{\partial x_m} \frac{\partial \eta}{\partial x_n} - c^2 (g_{mn} - B_{ijmn} \sigma_{ij}) \frac{\partial^2 \eta}{\partial x_m \partial x_n} + \frac{c^2 w_{ijkl} \partial^4 \eta}{\partial x_i \partial x_j \partial x_k \partial x_l} = 0, \quad (2a)$$

$$V_{ij} c + \frac{B_{ijmn}}{2} c^2 \frac{\partial \eta}{\partial x_m} \frac{\partial \eta}{\partial x_n} + s_{ijkl} \sigma_{kl} = u_{ij}. \quad (2b)$$

Here we used the identity,  $\operatorname{arctanh}(\eta) \equiv \frac{1}{2} \ln \left( \frac{1+\eta}{1-\eta} \right)$ .

Eq. (2) should be considered along with the conditions of mechanical equilibrium  $\partial \sigma_{ij} / \partial x_j = 0$ . The boundary conditions to Eqs. (2) are the following:

$$\sigma_{i3}(0) = 0, \quad u_{11}(h) = u_{22}(h) = u_m, \quad \text{and} \quad \left[ \alpha_s \eta \pm g c^2 \frac{\partial \eta}{\partial z} \mp B_{ij33} \sigma_{ij} c^2 \frac{\partial \eta}{\partial z} \right]_{x_3=0,h} = 0. \quad (2c)$$

Here  $u_m$  is a misfit strain induced by the film-substrate lattices mismatch. Below we consider thicknesses  $h$  smaller than the critical thickness of misfit dislocation appearance [40], typically this means that  $h \leq 10$  nm. Note that natural boundary conditions correspond to the case  $\alpha_s = 0$ .

The nonlinear boundary problem (2) contains a number of materials-dependent constants, the majority of which are poorly known even for simple binary oxides, such as ZnO, MgO, SnO<sub>2</sub>, CeO<sub>2</sub>, HfO<sub>2</sub>, and even more so for complex ternary oxides, such as manganites (La,Sr)MnO<sub>3</sub>, paraelectric perovskites SrTiO<sub>3</sub>, EuTiO<sub>3</sub>, KTaO<sub>3</sub>, ferroelectric perovskites (Ba,Sr)TiO<sub>3</sub>, (Pb,Zr)TiO<sub>3</sub>, and orthoferrites PbFeO<sub>3</sub>, pristine and rare-earth doped BiFeO<sub>3</sub>, etc., which all can be deficient in oxygen. Hence, priory to study the boundary problem (2) by e.g. finite element modeling (**FEM**), requiring all tabulated parameters taken from the experimental or density functional studies [5, 6, 8, 19]. However, to facilitate the search in the multi-parameter space and open the way for further FEM, here we elaborate the analytical theory.

### III. ANALYTICAL SOLUTION IN HARMONIC APPROXIMATION

To explore the phase evolution in the system described by free energy Eq. (1), we consider the three-dimensional Fourier series of the order parameter,

$$\eta(\mathbf{x}) = \sum_{l,m,n=-\infty}^{\infty} \tilde{\eta}_{lmn} \exp[i(k_1^{(lmn)}x_1 + k_2^{(lmn)}x_2 + k_3^{(lmn)}x_3)], \quad (3a)$$

where the wave vector components  $\mathbf{k}^{lmn} = \left(\frac{2\pi}{L}l, \frac{2\pi}{L}m, \frac{2\pi}{h}n\right)$  are determined by the sizes  $L \times L \times h$  of considered film, and  $m$ ,  $n$ , and  $l$  are integer numbers. For the order parameter  $\eta(\mathbf{x})$  to be a real (i.e. observable) value, the equality  $\tilde{\eta}_{l,m,n}^* = \tilde{\eta}_{-l,-m,-n}$  should be valid.

Following Landau theory, below we assume that only one principal mode  $\mathbf{k}$  dominates near the order-disorder phase transition,

$$\eta(\mathbf{x}) \cong \eta_0 + \tilde{\eta} \exp(i\mathbf{k}\mathbf{x}) + c.c. \equiv \eta_0 + 2|\tilde{\eta}| \cos[(\mathbf{k}\mathbf{x} + \delta)], \quad (3b)$$

where  $\delta$  is the phase shift and  $\eta_0$  is the offset term. Next, we assume that the approximate equality is valid for the order parameter derivative in Eq. (1c), namely:

$$\frac{\partial \eta}{\partial x_m} \frac{\partial \eta}{\partial x_n} = 2k_m k_n |\tilde{\eta}|^2 (1 - \cos[2(\mathbf{k}\mathbf{x} + \delta)]) \quad (3c)$$

Note that  $\mathbf{k}$  is constant in the first harmonic approximation, but should be found in the self-consistent way in what follows.

Substitution of Eqs. (3) in Eqs. (1b) and (1c) yields:

$$\frac{g_{ij}c^2}{2} \frac{\partial \eta}{\partial x_i} \frac{\partial \eta}{\partial x_j} \cong c^2 \tilde{g} |\tilde{\eta}|^2 (1 - \cos[2(\mathbf{k}\mathbf{x} + \delta)]), \quad \text{where} \quad \tilde{g}(\mathbf{k}) = g_{ij} k_i k_j, \quad (4a)$$

$$\frac{B_{ijmn}}{2} \sigma_{ij} c^2 \frac{\partial \eta}{\partial x_m} \frac{\partial \eta}{\partial x_n} \approx c^2 \tilde{B}_{ij}(\mathbf{k}) \sigma_{ij} |\tilde{\eta}|^2 (1 - \cos[2(\mathbf{k}\mathbf{x} + \delta)]), \quad \text{where} \quad \tilde{B}_{ij}(\mathbf{k}) = B_{ijmn} k_m k_n. \quad (4b)$$

$$\frac{w_{ijkl}c^2}{2} \frac{\partial^2 \eta}{\partial x_i \partial x_j} \frac{\partial^2 \eta}{\partial x_k \partial x_l} \cong c^2 \tilde{w} |\tilde{\eta}|^2 (1 + \cos[2(\mathbf{k}\mathbf{x} + \delta)]), \quad \text{where} \quad \tilde{w}(\mathbf{k}) = w_{ijkl} k_i k_j k_m k_n, \quad (4c)$$

Symmetry of the gradient-striction tensor  $B_{ijkl}$  is determined by the local site symmetry of defect planes with respect to the lattice. Below we assume the tetragonal symmetry of the tensor  $\tilde{B}_{ij}(\mathbf{k})$ , with a tetragonal axis along  $x_3$  axis of the film.

In the continuous media approximation the thermodynamically stable state of the film can be analyzed from the variation of the free energy (1) that acquires the form:

$$F = \int_{V_f} d\mathbf{x} \left[ \begin{aligned} & \frac{\alpha}{2} c^2 \eta^2 + c \frac{k_B T}{2} [(1-\eta)\ln(1-\eta) + (1+\eta)\ln(1+\eta)] - V_{ij} \sigma_{ij} c - \frac{s_{ijkl}}{2} \sigma_{ij} \sigma_{kl} + u_{kl} \sigma_{kl} \\ & + c^2 \tilde{g}(\mathbf{k}) |\tilde{\eta}|^2 (1 - \cos[2(\mathbf{k}\mathbf{x} + \delta)]) + c^2 \tilde{w}(\mathbf{k}) |\tilde{\eta}|^2 (1 + \cos[2(\mathbf{k}\mathbf{x} + \delta)]) \\ & - c^2 \tilde{B}_{ij}(\mathbf{k}) \sigma_{ij} |\tilde{\eta}|^2 (1 - \cos[2(\mathbf{k}\mathbf{x} + \delta)]) \end{aligned} \right] \quad (5a)$$

As a next step, one can use a Galerkin procedure in the free energy (5a) with respect to the second harmonics assuming statistical averaging, equivalent to the spatial averaging in ergodic case. Such averaging “excludes” the contribution from the second and higher harmonics to  $\cos[2(\mathbf{k}\mathbf{x} + \delta)]^{2n+1}$  due to a periodicity of trigonometric functions. Assuming the absence of correlations between the offset term  $\eta_0$  and  $\cos[2(\mathbf{k}\mathbf{x} + \delta)]$ , all cross-terms proportional to  $\eta_0^{2m+1} \cos[2(\mathbf{k}\mathbf{x} + \delta)]^{2n+1}$  vanish after the averaging. Next, the terms proportional to  $\eta_0^{2m+1}$  also vanish, while the even terms  $\eta_0^{2m}$  do not contain any useful information about defect ordering. Thus one can regard that  $\langle \eta^2 \rangle \sim |\tilde{\eta}|^2 \sim \eta^2$ , where the brackets  $\langle \dots \rangle$  designate the averaging, and obtain:

$$\begin{aligned} \langle f \rangle \sim c^2 & \left[ \frac{\alpha}{2} + \tilde{g} + \tilde{w} - \tilde{B}_{ij} \sigma_{ij} \right] \eta^2 + c \frac{k_B T}{2} [(1-\eta)\ln(1-\eta) + (1+\eta)\ln(1+\eta)] \\ & - V_{ij} \sigma_{ij} c - \frac{s_{ijkl}}{2} \sigma_{ij} \sigma_{kl} + u_{kl} \sigma_{kl} \end{aligned} \quad (5b)$$

Minimization of (5b),  $\frac{\partial \langle f \rangle}{\partial \eta} = 0$  and  $\frac{\partial \langle f \rangle}{\partial \sigma_{ij}} = 0$ , instead of Euler-Lagrange Eqs. (2), yields the algebraic equations of state:

$$c(\alpha + 2\tilde{g} + 2\tilde{w} - 2\tilde{B}_{ij} \sigma_{ij})\eta + k_B T \operatorname{arctanh}(\eta) = 0, \quad (6a)$$

$$V_{ij} c + \tilde{B}_{ij} c^2 \eta^2 + s_{ijkl} \sigma_{kl} = u_{ij}, \quad (6b)$$

Near the phase transition,  $\operatorname{arctanh}(\eta) \equiv \eta + \frac{\eta^3}{3}$  and Eq. (6a) can be rewritten as

$$c(\alpha + 2\tilde{g} + 2\tilde{w} - 2\tilde{B}_{ij} \sigma_{ij})\eta + k_B T \left( \eta + \frac{\eta^3}{3} \right) \approx 0 \quad (6c)$$

For simplicity, we consider the rotationally-isotropic Vegard effect,  $V_{ij} = V_m \delta_{ij}$ , where  $V_m$  is the partial molar volume. Using this approximation, elastic solution for a thin oxide film

on a rigid substrate is derived for cubic symmetry far from the structural domain walls. Zero components are  $\sigma_{33} = \sigma_{13} = \sigma_{23} = \sigma_{12} = 0$ ,  $u_{12} = u_{13} = u_{23} = 0$ , and nonzero components are:

$$\sigma_{11} = \frac{u_m - V_m c}{s_{11} + s_{12}} - \frac{s_{11} \tilde{B}_{11} - s_{12} \tilde{B}_{22}}{s_{11}^2 - s_{12}^2} c^2 \eta^2, \quad (7a)$$

$$\sigma_{22} = \frac{u_m - V_m c}{s_{11} + s_{12}} - \frac{s_{11} \tilde{B}_{22} - s_{12} \tilde{B}_{11}}{s_{11}^2 - s_{12}^2} c^2 \eta^2, \quad (7b)$$

$$u_{11} = u_{22} = u_m, \quad u_{33} = V_m c + \tilde{B}_{33} c^2 \eta^2 + \frac{s_{12}}{s_{11} + s_{12}} \left[ 2(u_m - V_m c) - (\tilde{B}_{11} + \tilde{B}_{22}) c^2 \eta^2 \right], \quad (7c)$$

Here  $u_m$  is a film-substrate lattices misfit strain. The convolutions  $\tilde{B}_{11} = B_{11} k_1^2 + B_{12} (k_2^2 + k_3^2)$ ,  $\tilde{B}_{22} = B_{11} k_2^2 + B_{12} (k_1^2 + k_3^2)$  and  $\tilde{B}_{33} = B_{11} k_3^2 + B_{12} (k_1^2 + k_2^2)$  are included in Eqs. (7), and the Voight notations for  $B_{1111} \equiv B_{11}$  and  $B_{1122} \equiv B_{12}$  are used hereinafter. In a freestanding film the stresses are zero  $\sigma_{ij} = 0$ , and elastic strains are  $u_{ij} = c V_m \delta_{ij} + \tilde{B}_{ij} c^2 \eta^2$ .

## IV. DEFECT ORDER-DISORDER TRANSITION

### A. Defect ordering parallel to the surface

Here we consider the case when the only nonzero component of wave vector is  $k_3$ , meaning that the defect-ordered layers are parallel to the film surfaces  $x_3=0, h$ . For the case the free energy density Eq. (1) has the following form:

$$f[\eta] = \alpha_p + \frac{\beta_{pr}}{2} c^2 \eta^2 + \frac{\gamma_{pr} c^4}{12} \eta^4 + c \frac{k_B T}{2} [(1-\eta) \ln(1-\eta) + (1+\eta) \ln(1+\eta)] \quad (8a)$$

Where the coefficients  $\alpha_p = \frac{(u_m - V_m c)^2}{s_{11} + s_{12}}$ ,  $\beta_{pr} = \alpha + 2(\tilde{g} + \tilde{w}) - \frac{4\tilde{B}_{22}(u_m - V_m c)}{s_{11} + s_{12}}$ ,  $\gamma_{pr} = \frac{12\tilde{B}_{22}^2}{s_{11} + s_{12}}$ ,

and  $\tilde{B}_{22} = B_{12} k_3^2$ ,  $\tilde{g} = g k_3^2$  and  $\tilde{w} = w k_3^4$ . We refer the case with subscript "pr".

Omitting  $\eta$ -independent term  $\alpha_{pr}$ , the free energy density (8a) can be expanded in power series in  $\eta$  as

$$\delta f[\eta] \approx (\beta_{pr} c^2 + c k_B T) \frac{\eta^2}{2} + \left( \frac{\gamma_{pr} c^4 + c k_B T}{3} \right) \frac{\eta^4}{4}. \quad (8b)$$

The derivation of Eqs. (8) is given in **Appendix A**. Note the renormalized coefficient before  $\eta^4$  should be positive to ensure the stability of the phase described by the free energy (8b), otherwise higher terms should be included. Since  $s_{11} > |s_{12}|$  for all elastically stable solids, and  $\tilde{B}_{22}^2 \geq 0$  the condition  $\gamma_{pr} \geq 0$  is always valid.

The equilibrium values of the order parameter obtained from minimization of the energy (8b) and the corresponding free energy have the form:

$$\eta_S^{pr} = \pm \sqrt{-3 \frac{\beta_{pr}c + k_B T}{\gamma_{pr}c^3 + k_B T}}, \quad \delta f_{pr}[\eta_S^{pr}] = -\frac{3c}{4} \frac{(\beta_{pr}c + k_B T)^2}{\gamma_{pr}c^3 + k_B T}. \quad (8c)$$

Long-range order exists if  $\beta_{pr}c + k_B T < 0$ .

### B. Defect ordering perpendicular to the surface

We further consider the case when the only nonzero component of the wave vector is  $k_1$ , meaning that the defect-ordered layers are perpendicular to the film surfaces  $x_3=0, h$ . The free energy density  $f$  in Eq. (1b) of the oxide has the following form in this case:

$$f[\eta] = \alpha_p + \frac{\beta_{pp}}{2} c^2 \eta^2 + \frac{\gamma_{pp} c^4}{12} \eta^4 + c \frac{k_B T}{2} [(1-\eta)\ln(1-\eta) + (1+\eta)\ln(1+\eta)] \quad (9a)$$

Where  $\beta_{pp} = \alpha + 2 \left( \tilde{g} + \tilde{w} - \frac{(\tilde{B}_{11} + \tilde{B}_{22})(u_m - V_m c)}{s_{11} + s_{12}} \right)$  and  $\gamma_{pp} = 6 \frac{(\tilde{B}_{11}^2 + \tilde{B}_{22}^2)s_{11} - 2\tilde{B}_{11}\tilde{B}_{22}s_{12}}{(s_{11}^2 - s_{12}^2)}$  with

$\tilde{B}_{11} = B_{11}k_1^2$ ,  $\tilde{B}_{22} = B_{12}k_1^2$ ,  $\tilde{g} = gk_1^2$  and  $\tilde{w} = wk_1^4$ . We denote this case with subscript "pp".

Omitting  $\eta$ -independent term  $\alpha_{pr}$ , the free energy density (9a) can be expanded in powers of  $\eta$  as

$$\delta f[\eta] \approx (\beta_{pp}c^2 + ck_B T) \frac{\eta^2}{2} + \left( \frac{\gamma_{pp}c^4 + ck_B T}{3} \right) \frac{\eta^4}{4}. \quad (9b)$$

Note the renormalized coefficient before  $\eta^4$  should be positive, otherwise higher terms should be included. Thus, the inequality  $\gamma_{pp}c^4 + ck_B T > 0$  should be verified. Since  $s_{11} > |s_{12}|$  for all elastically stable solids, and  $\tilde{B}_{11}^2 + \tilde{B}_{22}^2 \geq 2|\tilde{B}_{11}\tilde{B}_{22}|$  the condition  $\gamma_{pp} > 0$  is always valid, and so  $\gamma_{pp}c^4 + ck_B T > 0$  at finite temperatures.

The equilibrium values of the order parameter obtained from minimization of the energy (9b) and corresponding energy have the form similar to Eq. (8c):

$$\eta_S^{pp} = \pm \sqrt{-3 \frac{\beta_{pp}c + k_B T}{\gamma_{pp}c^3 + k_B T}}, \quad \delta f_{pp} [\eta_S^{pp}] = -\frac{3c (\beta_{pp}c + k_B T)^2}{4 (\gamma_{pp}c^3 + k_B T)}. \quad (9c)$$

Long-range order exists if  $\beta_{pp}c + k_B T < 0$ . The derivation of Eqs. (9) is given in **Appendix**.

Note, that in the ordered phases elastic dipoles can become polar due to the surface-induced piezoelectric coupling that in turn originates from the inversion symmetry breaking near the film surfaces. At the same time the out-of-plane polar phase is affected by the strong depolarization field originated from the sharp gradient of polarization decay away from the surfaces.

### C. Structural phase diagrams

The temperatures of transition between defect-disordered and defect-ordered phases for **parallel** and **perpendicular** orientations of defect planes can be determined from equations

$$T_{pp}[u_m, c, k_1] = -\frac{\beta_{pp}c}{k_B} \equiv -\frac{c}{k_B} \left( \alpha + 2(gk_1^2 + wk_1^4) - 2k_1^2 \frac{(B_{11} + B_{12})}{s_{11} + s_{12}} (u_m - V_m c) \right), \quad (10a)$$

$$T_{pr}[u_m, c, k_3] = -\frac{\beta_{pr}c}{k_B} \equiv -\frac{c}{k_B} \left( \alpha + 2(gk_3^2 + wk_3^4) - \frac{4k_3^2 B_{12}}{s_{11} + s_{12}} (u_m - V_m c) \right). \quad (10b)$$

We further explore the equilibrium period of defect density modulation, related to the wave vector  $\mathbf{k}$ . In equilibrium the conditions  $\frac{\partial T_{pp}}{\partial k_i} = \frac{\partial T_{pr}}{\partial k_i} = 0$  should be fulfilled [47]. Thus

$$\frac{\partial T_{pp}}{\partial k_1} = -\frac{4c}{k_B} k_1 \left( \left( g - \frac{(B_{11} + B_{12})(u_m - V_m c)}{s_{11} + s_{12}} \right) + 2wk_1^2 \right) = 0 \quad \text{for the defect-ordered layers}$$

$$\text{perpendicular to the film surfaces, and } \frac{\partial T_{pr}}{\partial k_3} = -\frac{4c}{k_B} k_3 \left( \left( g - \frac{2B_{12}(u_m - V_m c)}{s_{11} + s_{12}} \right) + 2wk_3^2 \right) = 0 \text{ for the}$$

defect-ordered layers parallel to the film surfaces.

From these conditions the components of the modulation vector acquire the form:

$$k_1 = \pm \sqrt{-\frac{1}{2w} \left( g - \frac{B_{11} + B_{12}}{s_{11} + s_{12}} (u_m - V_m c) \right)}, \quad k_3 = \pm \sqrt{-\frac{1}{2w} \left( g - \frac{2B_{12}(u_m - V_m c)}{s_{11} + s_{12}} \right)}. \quad (11)$$

It is instructive to rewrite and analyze expressions (11) in a dimensionless form, namely

$$\frac{k_1}{k_0} = \pm \sqrt{-\frac{g}{|g|} + b_1 u} \quad \text{and} \quad \frac{k_3}{k_0} = \pm \sqrt{-\frac{g}{|g|} + b_3 u}, \quad \text{where } k_0 = \sqrt{\frac{|g|}{2w}}$$

$u = u_m - V_m c$  is a dimensionless ‘‘effective’’ strain;  $b_1 = \frac{B_{11} + B_{12}}{|g|(s_{11} + s_{12})}$  and  $b_3 = \frac{2B_{12}}{|g|(s_{11} + s_{12})}$  are dimensionless gradient-related parameters. Below we will analyze the positive roots  $k_{1,3} > 0$  only, since the negative ones describe the same physical states.

**Figure 2** illustrates the square-root like dependences of the dimensionless wave-vector components,  $k_1/k_0$  and  $k_3/k_0$ , on the effective strain  $u$  for  $g > 0$  (red and magenta curves) and  $g < 0$  (black and blue curves). Note that positive  $w$  determines the existence of the modulation and its characteristic wave number.

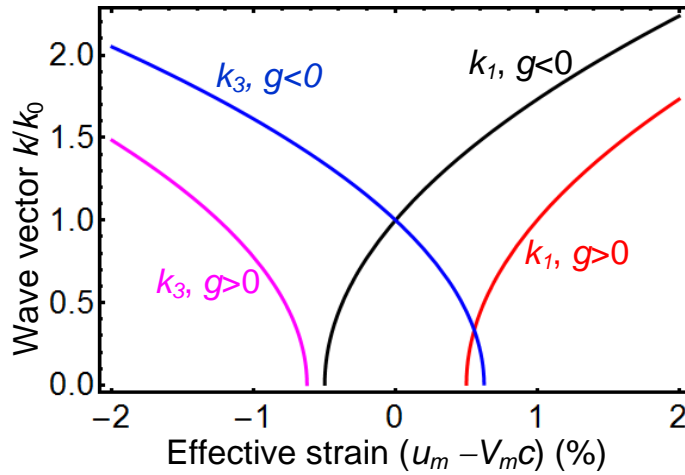


**FIGURE 2.** The dependence of the wave-vector component  $k_1/k_0$  and  $k_3/k_0$  on the effective strain  $u_m - V_m c$  calculated from Eqs. (11) for  $g > 0$  (red and magenta curves) and  $g < 0$  (black and blue curves), parameters  $b_1 = 200$  and  $b_3 = -160$ .

The transition temperatures, corresponding to the defect spatial modulation vectors given by Eq. (11), are

$$T_{pp}(u_m, c) = -\frac{c}{k_B} \left( \alpha - \frac{1}{2w} \left( g - \frac{B_{11} + B_{12}}{s_{11} + s_{12}} (u_m - V_m c) \right)^2 \right) \quad (12a)$$

$$T_{pr}(u_m, c) = -\frac{c}{k_B} \left( \alpha - \frac{1}{2W} \left( g - \frac{2B_{12}}{s_{11} + s_{12}} (u_m - V_m c) \right) \right)^2 \quad (12b)$$

The conditions of the equilibrium between the ordered phases can be obtained from the equality of the corresponding free energy densities, Eqs. (8c) and (9c), namely

$$\frac{(\beta_{pr}c + k_B T)^2}{\gamma_{pr}c^3 + k_B T} = \frac{(\beta_{pp}c + k_B T)^2}{\gamma_{pp}c^3 + k_B T}, \quad (13a)$$

allowing for the conditions of the long-range orders existence

$$\beta_{pr}c + k_B T < 0, \quad \beta_{pp}c + k_B T < 0. \quad (13b)$$

Note that the expressions (11) for  $\mathbf{k}$ -vector components should be substituted in Eqs. (13).

Equation (13a) can be solved with respect to temperature in the following form:

$$T = \frac{c}{k_B} \frac{(\beta_{pr}^2 - \beta_{pp}^2) + 2c^2(\beta_{pr}\gamma_{pp} - \beta_{pp}\gamma_{pr}) \pm \text{Det}[\beta_{pp}, \beta_{pr}]}{4(\beta_{pp} - \beta_{pr}) - 2(\gamma_{pp} - \gamma_{pr})c^2}, \quad (14a)$$

$$\text{Det}[\beta_{pp}, \beta_{pr}] = \sqrt{(\beta_{pp} - \beta_{pr})^4 + 4(\beta_{pp} - \gamma_{pp}c^2)(\beta_{pr} - \gamma_{pr}c^2)(\beta_{pp} - \beta_{pr})^2}. \quad (14b)$$

The signs “ $\pm$ ” in Eq.(14a) correspond to two different roots, which should have physical sense, i.e. correspond to  $T \geq 0$ . These roots should further satisfy two conditions (13b). Depending on the parameters it appeared possible at least for the largest root of Eq. (14a). Since the sign of denominator in Eq. (14a) is not fixed, both signs in the numerator,  $+\text{Det}[\beta_{pp}, \beta_{pr}]$  or  $-\text{Det}[\beta_{pp}, \beta_{pr}]$ , are possible depending on the parameters. Hence, the number and selection of the roots in Eqs. (14) should be established numerically depending on the number and values of the fitting parameters.

It can be shown that, at the chosen parameter values, one of the roots (14a) is close to the expression  $(T_{pp}(u_m, c) + T_{pr}(u_m, c))/2$ . Hence, for  $\beta_{pp} \approx \beta_{pr}$  expression (14) can be expanded in series on the small difference  $(\beta_{pp} - \beta_{pr})$  powers, namely

$$T \approx \frac{c}{k_B} (\beta_{pp} - \beta_{pr}) \left( -\frac{1}{2} + \frac{\gamma_{pp}c^2 - \beta_{pp} \pm \sqrt{(\gamma_{pp}c^2 - \beta_{pp})(\gamma_{pr}c^2 - \beta_{pr})}}{(\gamma_{pp} - \gamma_{pr})c^2} \right). \text{ When the strong inequality}$$

$|\gamma_{pp} - \gamma_{pr}| \ll \gamma_{pp}$  takes place, the second term in parenthesis could be either close to unity (sign “-“) or much higher than unity (sign “+“). It is seen that in the case of “-“ the solution (14b) will not satisfy both of relations (13b) simultaneously. The other root in Eq. (14c) deviates more

significantly from the value  $[T_{pp}(u_m, c) + T_{pr}(u_m, c)]/2$ , thus, in this case, conditions (13b) will be satisfied.

Using Eqs. (10)-(14) we plotted phase diagrams of the system and corresponding modulation amplitudes and wave vectors, shown in **Fig. 3-4** and **Fig. 5**, respectively. Note that the ordered phases  $OP_{\perp}$  and  $OP_{\parallel}$  have different orientation of the order parameter modulation amplitude,  $\eta(x)$  and  $\eta(z)$ , with respect to the film surfaces. **Fig. 3(a)** represents the scheme of the defects distribution in the ordered ( $OP_{\perp}$  and  $OP_{\parallel}$ ) and disordered (DP) phases.

**Figures 3b-e** and **4a-d** are phase diagrams of an ultra-thin film in dependence on misfit strain  $u_m$  and dimensionless defect concentration  $c/c_0$  calculated for negative and positive  $\alpha$ , respectively. Corresponding modulation wave vectors,  $k_{\perp}$  and  $k_{\parallel}$ , are shown in **Figs. 5a** and **5b**, respectively.

**Figures 3(b-e)**, calculated for negative  $\alpha$ , demonstrate the presence of  $OP_{\perp}$ ,  $OP_{\parallel}$  and DP phases, whose boundaries depend on the gradient  $g$  and striction  $B_{ij}$  coefficients, which are different for **Figs. 3(b-e)**. The thin almost vertical dark green stripe between  $OP_{\parallel}$  and  $OP_{\perp}$  phases located at small  $|u_m| < 0.1\%$  in **Fig. 3b** and **3c** is the homogeneously ordered phase, i.e.  $\eta = \text{const}$ , and  $\mathbf{k} = 0$ . This phase is absent for the diagrams in **Figs. 3d** and **3e**, which have a tricritical point, where  $OP_{\perp}$ ,  $OP_{\parallel}$  and DP phases coexist. The tricritical point  $\{u_m = 0, c/c_0 = 0.63\}$  is almost independent on  $g$  and  $B_{ij}$  signs. The  $OP_{\parallel}$ -DP and  $OP_{\perp}$ -DP boundaries are curved for all diagrams. DP phase occupies mountain-shape region with the “top” at  $\{u_m = 0, c/c_0 = 0.63\}$ , which hill-sides start at small misfits. The region of its stability gradually decreases with  $|u_m|$  increase. At that the noticeable asymmetry between compressive ( $u_m < 0$ ) and tensile ( $u_m > 0$ ) misfit strains are evident and related with positive Vegard effect ( $V_m > 0$ ). It can be deduced from **Fig. 3(b-e)**, that the change of the  $B_{ij}$  sign leads to an interchange between the  $OP_{\parallel}$  and  $OP_{\perp}$  phases with different orientation of  $\eta$ -ordering, stemming from the chemo-strictive coupling between the strain  $u_m$  and defect concentration  $c$ , expressed by the coupling terms  $\frac{B_{11} + B_{12}}{s_{11} + s_{12}}(u_m - V_m c)$  and

$$\frac{2B_{12}}{s_{11} + s_{12}}(u_m - V_m c).$$

The  $OP_{\parallel}$ - $OP_{\perp}$  boundary is almost vertical, and its small slope weakly depends on the  $V_m$  value. The  $OP_{\perp}$  phase exists for compressive misfit strain  $u_m < 0$  at  $B_{11} + B_{12} < 0$ , and for tensile misfit strain  $u_m > 0$  at  $B_{11} + B_{12} > 0$ . The  $OP_{\parallel}$  phase exists for compressive misfit strain  $u_m < 0$  at  $B_{11} + B_{12} > 0$ , and for tensile misfit strain  $u_m > 0$  at  $B_{11} + B_{12} < 0$ . The color maps of the order parameter amplitudes [ $\eta(x_1)$  and  $\eta(x_3)$ ] and wave vectors ( $k_{\perp}$  and  $k_{\parallel}$ ) calculated for  $\alpha < 0$ ,  $g > 0$ ,  $B_{11} + B_{12} > 0$  are shown in **Figs. 5a** and **5c**, respectively. The continuous transition from  $OP_{\parallel}$  to  $OP_{\perp}$  phase occurs at  $u_m = 0$ . Notably that  $k_{\perp}=k_{\parallel}=0$  in the region  $u_m \approx 0$ . The values of  $\eta$  and  $k$  gradually increase with  $|u_m|$  increase.

The change of  $\alpha$  sign critically affects the phase diagrams, as shown in **Fig. 4**. The most pronounced effect is the appearance of the wide DP region between the ordered  $OP_{\perp}$  and  $OP_{\parallel}$  phases, so that the tricritical point is absent for all concentrations. Note that the DP exist in the regions of misfits  $|u_m| \leq 2\%$  and this region grows with defect concentration decrease. The width of DP region slightly increases with  $|u_m|$  increase. The change of the  $B_{ij}$  sign leads to the interchange between the  $OP_{\parallel}$  and  $OP_{\perp}$  phases, while the effect of the coefficient  $g$  is negligibly small in this case [compare **Figs. 4a-b** with **4c-d**]. The  $OP_{\perp}$  phase exists for high compressive misfit strain  $u_m < -2.5\%$  at  $B_{11} + B_{12} < 0$ , and for tensile misfit strain  $u_m > +2.5\%$  at  $B_{11} + B_{12} > 0$ . The  $OP_{\parallel}$  phase exists for compressive misfit strain  $u_m < -1.9\%$  at  $B_{11} + B_{12} > 0$ , and for tensile misfit strain  $u_m > +1.9\%$  at  $B_{11} + B_{12} < 0$ . The color maps of the order parameter amplitudes [ $\eta(x_1)$  and  $\eta(x_3)$ ] and wave vectors ( $k_{\perp}$  and  $k_{\parallel}$ ) calculated for  $\alpha > 0$ ,  $g > 0$ ,  $B_{11} + B_{12} > 0$  are shown in **Figs. 5b** and **5d**, respectively. The  $OP_{\parallel}$  to  $OP_{\perp}$  phases are separated by a wide region of DP phase located at  $|u_m| \leq 2\%$ . The values of  $k$  are nonzero at the DP- $OP_{\parallel}$  and DP- $OP_{\perp}$  boundaries. The values of  $\eta$  and  $k$  gradually increase with  $|u_m|$  increase.

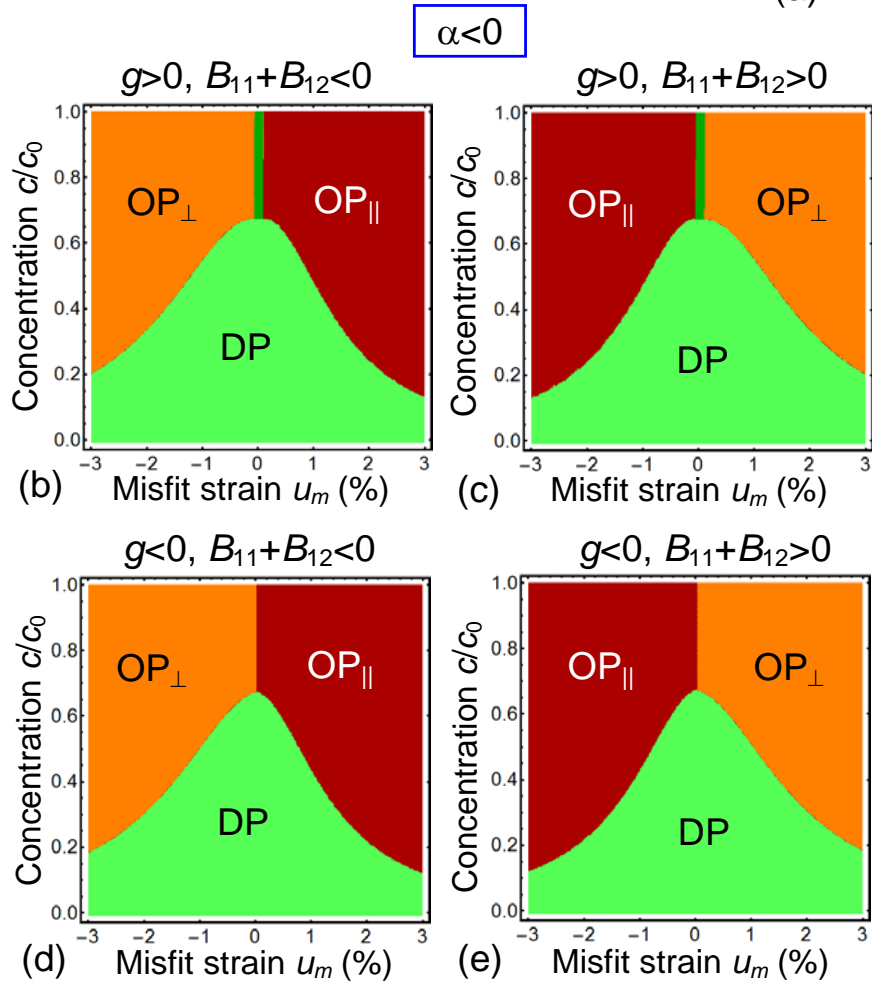
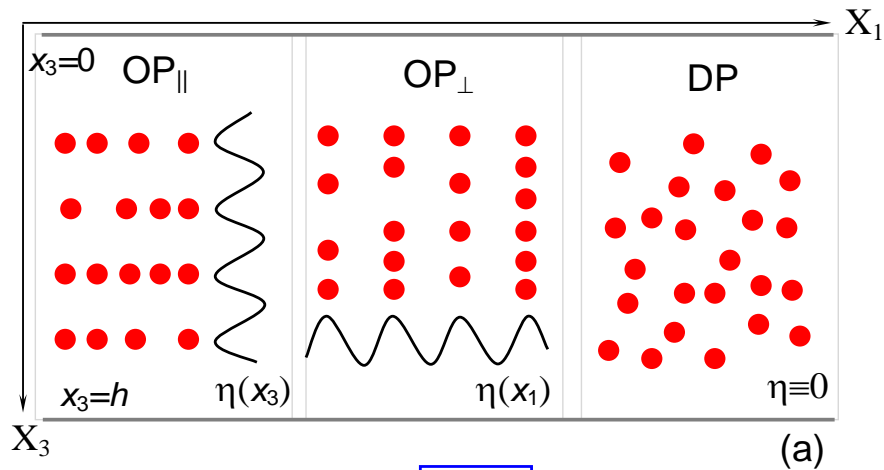


**FIGURE 3.** (a) Geometry of the problem and schematics of different phases characterized by different degree of ordering. Here we show the disordered phase DP, the  $OP_{\perp}$  phase with defect layers perpendicular to the substrate plane and the  $OP_{\parallel}$  phase with defect layers parallel to the substrate plane. (b)-(e) Phase diagrams in dependence on normalized defect concentration  $c/c_0$  and misfit strain  $u_m$  calculated for negative  $\alpha$ , different signs of coefficient  $g$  and striction coefficients  $B_{ij}$  (indicated above the

plots) at room temperature  $T=293$  K. Parameters:  $\alpha c_0^2 = -6 \times 10^4$  J·m<sup>-3</sup>,  $|g|c_0^2 = 10^{-17}$  J/m,  $wc_0^2 = 3 \times 10^{-37}$  J·m,  $s_{11} = 4 \times 10^{-12}$  Pa<sup>-1</sup>,  $s_{12} = -1 \times 10^{-12}$  Pa<sup>-1</sup>,  $V_m = 30$  Å<sup>3</sup>, while striction coefficients  $B_{11}c_0^2 = 5 \times 10^{-26}$  J·m<sup>2</sup>, and  $B_{12}c_0^2 = -2 \times 10^{-26}$  J·m<sup>2</sup>, and maximal (steric limit) concentration of defects is  $c_0 = 10^{25}$  m<sup>-3</sup>.

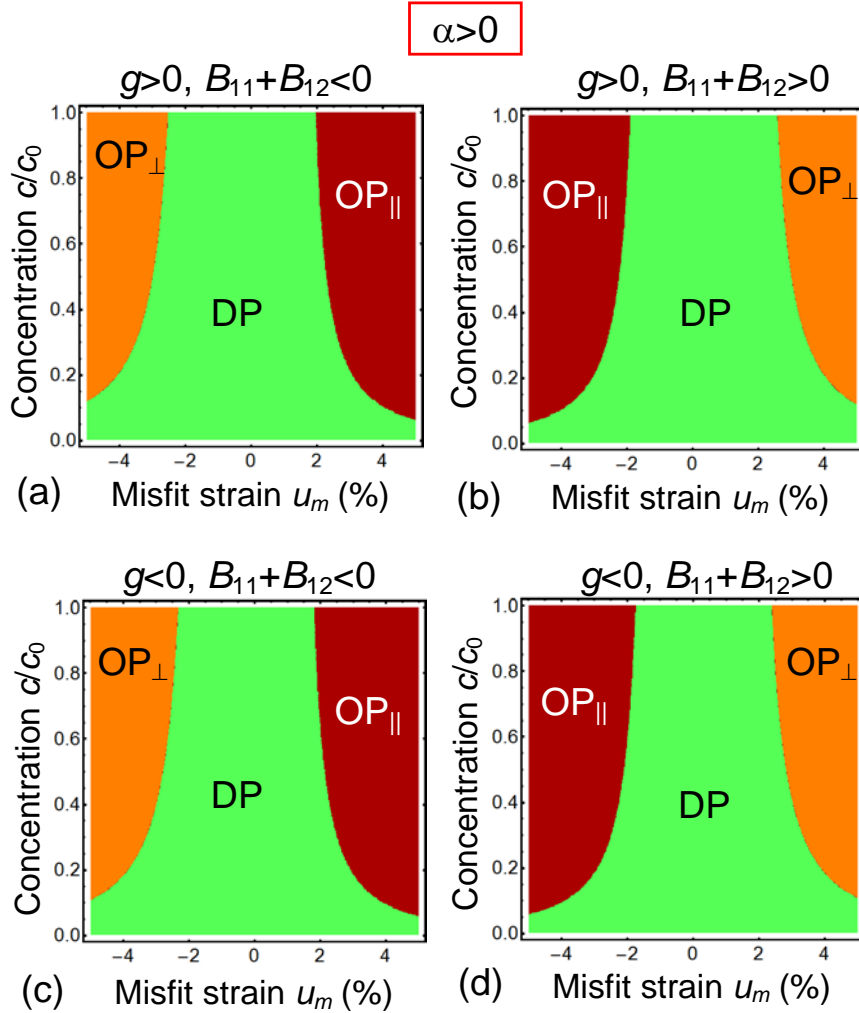


**FIGURE 4.** Phase diagrams in dependence on normalized defect concentration  $c/c_0$  and misfit strain  $u_m$  calculated for positive  $\alpha$ , different signs of gradient coefficient  $g$  and striction coefficients  $B_{ij}$  (indicated above the plots), and  $\alpha > 0$ . Other parameters are the same as in **Fig. 3**.

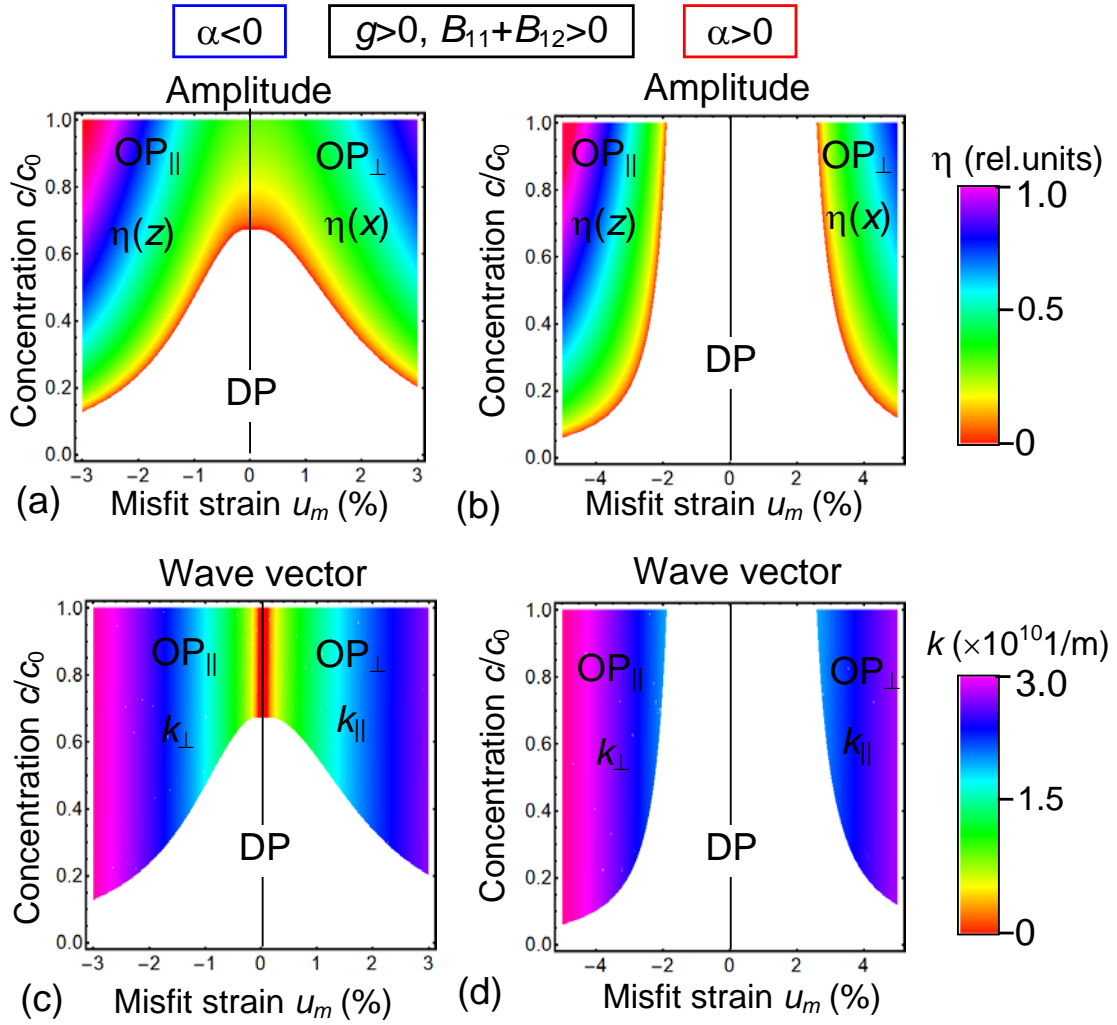


**FIGURE 5.** Order parameter amplitudes  $\eta(x_1)$  and  $\eta(x_3)$  **(a, b)** and wave vectors **(c, d)** in dependence on normalized defect concentration  $c/c_0$  and misfit strain  $u_m$  calculated for negative  $\alpha$  **(a, c)** and positive  $\alpha$  **(b, d)**;  $g > 0 \text{ J}\cdot\text{m}^5$ , and  $B_{11} + B_{12} > 0$ . Numerical values of parameters are the same as in **Fig. 3**.

Note that phenomenological parameters listed in the caption to **Fig. 3** were selected in such way to satisfy the physical conditions  $\alpha c_0 \cong k_B T_{room}$ ,  $\sqrt{|\alpha|/g} \geq k_0$ ,  $\sqrt{|g|/w} < k_0$ ,  $s_{ij}$  and  $c_0$  values are typical for oxides. As for the striction coefficients  $B_{ij}$ , these are chosen so that the combinations of parameters,  $\frac{B_{11} + B_{12}}{s_{11} + s_{12}}(u_m - V_m c)$  and  $\frac{2B_{12}}{s_{11} + s_{12}}(u_m - V_m c)$ , are of the same order as  $|g|$ . To summarize the section, results shown in **Fig. 3-5** indicate that one can control the

defect ordering-disordering by changing their concentration  $c/c_0$  and misfit strain  $u_m$  at fixed other parameters.

## V. DISCUSSION

Here we briefly discuss several specific aspects of the defect ordering in ultra-thin oxide films on a substrate, which thicknesses is smaller than the critical thickness of misfit dislocation appearance, namely with  $h \leq 10$  nm (see **Section II**). Given that oxygen vacancies are elastic dipoles characterized by the stress tensor  $\sigma_{ij}$ , we can suppose that parallel defect planes depicted in **Fig. 1** produce in-plane strains only. On the other hand, perpendicular defect planes can produce out-of-plane strains, and are occupied by electric dipoles  $d_3$  originated from surface-induced piezoelectric effect characterized by piezoelectric tensor  $d_{ij3}$ , so that  $d_3 = d_{ij3}\sigma_{ij}$ . Therefore we can observe a coexistence of elastic and electric dipoles, which ordering, structural phase diagrams and transition temperatures are calculated analytically in **Section III** and analyzed graphically in **Section IV**. Note that the disordered phase is also present at the phase diagrams, occupying the regions of small misfits and defect concentrations. Hence, the detailed study of ultra-thin films paves the way to essential progress both in fundamental physics and applications in the near future of nanostructured materials, where the influence of surface is decisive.

## VI. CONCLUSION

We have analyzed the ordering of defects (e.g. oxygen vacancies) in thin oxide films In the framework of the continuum Landau-type theory. We derived analytical expressions for the energies of various defect-ordered states and calculated and analyzed phase diagrams dependence on the film-substrate misfit strain and concentration of defects for different gradient, striction and Vegard coefficients.

We have found that two defect-ordered phases, which are characterized by either parallel or perpendicular defect ordering in planes and corresponding wave vectors, can be stable. The stability conditions are determined by the misfit strain and the defect concentration at fixed other parameters. The ordered phases border with the defect-disordered phase. Hence, we have shown that one can control the defect ordering-disordering by changing their concentration and the film-substrate misfit strain (compressive or tensile). Thus the obtained results open possibilities to

create and control superstructures of ordered defects in thin oxide films by selecting the appropriate substrate and defect concentration.

**Acknowledgements.** This material is based upon work (S.V.K.) supported by the U.S. Department of Energy, Office of Science, Office of Basic Energy Sciences, and performed in the Center for Nanophase Materials Sciences, supported by the Division of Scientific User Facilities. This work was supported by the Deutsche Forschungsgemeinschaft (DFG) via the grant No. 405631895 (GE-1171/8-1). A portion of FEM was conducted at the Center for Nanophase Materials Sciences, which is a DOE Office of Science User Facility (CNMS Proposal ID: 257). M.V.S. also acknowledges Russian academic excellence project "5-100" for Sechenov University.

### APPENDIX. Derivation of Free Energy Expression

Let us denote the amplitude of concentration modulation as  $\eta$ , and wave vector of modulation as  $k_i$ , where  $i=1, 2, 3$  denotes different components of vector, determining the orientations of ordering (modulation) planes, so that we suppose the following distribution of defects (spatial profile of the concentration):

$$n = c(\eta_0 + \tilde{\eta} \exp[i(k_1x_1 + k_2x_2 + k_3x_3)] + c. c.) \quad (\text{A.1})$$

Correspondingly, the gradient of the concentration is

$$\frac{\partial n}{\partial x_j} = ik_j c \tilde{\eta} \exp[i(k_1x_1 + k_2x_2 + k_3x_3)] + c. c. \quad (\text{A.2})$$

One could easily find from (A.1) and (A.2) the mean square average of the concentration gradient

$$\left\langle \frac{\partial n}{\partial x_i} \frac{\partial n}{\partial x_j} \right\rangle \cong 2c^2 |\tilde{\eta}|^2 k_i k_j \quad (\text{A.3})$$

Note, that harmonic functions disappeared after the averaging.

General expression for concentration gradient contribution the free energy density is

$$\frac{g_{ij}}{2} \frac{\partial n}{\partial x_i} \frac{\partial n}{\partial x_j} + B_{ijkl} \frac{\sigma_{ij}}{2} \left( \frac{\partial n}{\partial x_k} \frac{\partial n}{\partial x_l} + \frac{\partial n}{\partial x_l} \frac{\partial n}{\partial x_k} \right) \quad (\text{A.4})$$

Using expressions (A.1)-(A.4) different contributions to the free energy of the system could be written as follows:

$$\left\langle g_{ij} \frac{\partial n}{\partial x_i} \frac{\partial n}{\partial x_j} \right\rangle \cong 2g_{ij} k_i k_j c^2 |\tilde{\eta}|^2 \quad (\text{A.5})$$

$$\langle B_{ijkl} \sigma_{ij} \frac{\partial n}{\partial x_k} \frac{\partial n}{\partial x_l} \rangle = 2c^2 B_{ijkl} k_i k_j |\tilde{\eta}|^2 \sigma_{ij}, \quad (\text{A.6})$$

Taking into account (A.5)-(A.6) and using isotropic approximation,  $g_{ij} = g\delta_{ij}$ , the gradient and elastic contributions of free energy can be expanded on the powers of  $k_i$ . Result has the following form

$$\begin{aligned} \Delta F_{FE} = & gc^2(k_1^2 + k_2^2 + k_3^2)|\tilde{\eta}|^2 - B_{11}c^2(\sigma_{11}k_1^2 + \sigma_{22}k_2^2 + \sigma_{33}k_3^2)|\tilde{\eta}|^2 \\ & - B_{12}c^2(\sigma_{11}k_2^2 + \sigma_{22}k_1^2 + \sigma_{11}k_3^2 + \sigma_{33}k_1^2 + \sigma_{22}k_3^2 + \sigma_{33}k_2^2)|\tilde{\eta}|^2 \\ & - B_{44}c^2(\sigma_{12}k_1k_2 + \sigma_{13}k_1k_3 + \sigma_{23}k_2k_3)|\tilde{\eta}|^2 - \frac{S_{11}}{2}(\sigma_{11}^2 + \sigma_{22}^2 + \sigma_{33}^2) \\ & - s_{12}(\sigma_{11}\sigma_{22} + \sigma_{11}\sigma_{33} + \sigma_{22}\sigma_{33}) - \frac{S_{44}}{2}(\sigma_{12}^2 + \sigma_{13}^2 + \sigma_{23}^2) \\ & - c\beta_{11}(\sigma_{11} + \sigma_{22} + \sigma_{33}) \end{aligned} \quad (\text{A.7})$$

Voight matrix notations is used in Eq.(A.7), and  $B_{ij}$  are the components of the fourth rank tensor in these notations, which are different from the second rank tensor,  $\tilde{B}_{ij}$ , introduced in the main text. Voight notations are

$$s_{1111} = s_{11}, \quad s_{1122} = s_{12}, \quad 4s_{1212} = s_{44}, \quad (\text{A.8})$$

$$B_{1111} = B_{11}, \quad B_{1122} = B_{12}, \quad 4B_{1212} = B_{44}, \quad (\text{A.9})$$

Modified Hooke's law could be obtained from the relation  $u_{ij} = -\partial(\Delta F_{FE})/\partial \sigma_{ij}$ :

$$u_{11} = s_{11}\sigma_{11} + s_{12}\sigma_{22} + s_{12}\sigma_{33} + (B_{11}k_1^2 + B_{12}k_2^2 + B_{12}k_3^2)|\tilde{\eta}|^2 c^2 + V_{11}c, \quad (\text{A.10})$$

$$u_{22} = s_{12}\sigma_{11} + s_{11}\sigma_{22} + s_{12}\sigma_{33} + (B_{12}k_1^2 + B_{11}k_2^2 + B_{12}k_3^2)|\tilde{\eta}|^2 c^2 + V_{11}c, \quad (\text{A.11})$$

$$u_{33} = s_{12}\sigma_{11} + s_{12}\sigma_{22} + s_{11}\sigma_{33} + (B_{12}k_1^2 + B_{12}k_2^2 + B_{11}k_3^2)|\tilde{\eta}|^2 c^2 + V_{11}c, \quad (\text{A.12})$$

$$\begin{aligned} u_4 = s_{44}\sigma_{23} + B_{44}k_2k_3|\tilde{\eta}|^2 c^2, \quad u_5 = s_{44}\sigma_{13} + B_{44}k_1k_3|\tilde{\eta}|^2 c^2, \\ u_6 = s_{44}\sigma_{12} + B_{44}k_1k_2|\tilde{\eta}|^2 c^2 \end{aligned} \quad (\text{A.13})$$

The solution for the misfit of thin film with its substrate is well known. For the film with normal along  $X_3$  one has the following relations for some of stress and strain components:

$$\sigma_{13} = \sigma_{23} = \sigma_{33} = 0 \quad (\text{A.14})$$

$$u_{11} = u_m, \quad u_{22} = u_m, \quad u_6 = 0 \quad (\text{A.15})$$

Here  $u_m$  is the misfit strain. For the sake of simplicity let us consider the case of only one zero component,  $k_2 = 0$ . Therefore, taking (A.14) and (A.15) into account, one could rewrite (A.10)-(A.13) in the following form:

$$u_m = s_{11}\sigma_{11} + s_{12}\sigma_{22} + (B_{11}k_1^2 + B_{12}k_3^2)|\tilde{\eta}|^2 c^2 + V_{11}c \quad (\text{A.16a})$$

$$u_m = s_{12}\sigma_{11} + s_{11}\sigma_{22} + (B_{12}k_1^2 + B_{12}k_3^2)|\tilde{\eta}|^2 c^2 + V_{11}c \quad (\text{A.16b})$$

$$u_{33} = s_{12}\sigma_{11} + s_{12}\sigma_{22} + (B_{12}k_1^2 + B_{11}k_3^2)|\tilde{\eta}|^2c^2 + V_{11}c \quad (\text{A.16c})$$

$$u_4 = 0, u_5 = B_{44}k_1k_3|\tilde{\eta}|^2c^2, \sigma_{12} = 0. \quad (\text{A.16d})$$

The solution of the system (A.16) is

$$\begin{aligned} \sigma_{11} &= \frac{u_m - V_{11}c}{s_{11} + s_{12}} - \frac{B_{12}k_3^2|\tilde{\eta}|^2c^2}{s_{11} + s_{12}} - \frac{1}{2} \left( \frac{B_{11}k_1^2 + B_{12}k_1^2}{s_{11} + s_{12}} + \frac{B_{11}k_1^2 - B_{12}k_1^2}{s_{11} - s_{12}} \right) |\tilde{\eta}|^2c^2 \\ \sigma_{22} &= \frac{u_m - V_{11}c}{s_{11} + s_{12}} - \frac{B_{12}k_3^2|\tilde{\eta}|^2c^2}{s_{11} + s_{12}} - \frac{1}{2} \left( \frac{B_{11}k_1^2 + B_{12}k_1^2}{s_{11} + s_{12}} - \frac{B_{11}k_1^2 - B_{12}k_1^2}{s_{11} - s_{12}} \right) |\tilde{\eta}|^2c^2 \\ u_{33} &= s_{12} \frac{2u_m - (B_{11} + B_{12})k_1^2|\tilde{\eta}|^2c^2 - 2B_{12}k_3^2|\tilde{\eta}|^2c^2}{s_{11} + s_{12}} + (B_{12}k_1^2 + B_{11}k_3^2)|\tilde{\eta}|^2c^2 + \beta_{11}c \frac{s_{11} - s_{12}}{s_{11} + s_{12}} \\ \sigma_{12} &= 0, u_4 = 0, u_5 = B_{44}k_1k_3|\tilde{\eta}|^2c^2. \end{aligned} \quad (\text{A.17})$$

Finally, free energy renormalization could be obtained from the Legendre transformation of the initial free energy (A.7),  $\Delta\tilde{F}_{FE} = \Delta F_{FE} + \sigma_{11}u_{11} + \sigma_{22}u_{22}$ , that is:

$$\begin{aligned} \Delta\tilde{F}_{FE} &= gc^2(k_1^2 + k_3^2)|\tilde{\eta}|^2 - B_{11}(\sigma_{11}k_1^2)|\tilde{\eta}|^2c^2 - B_{12}(\sigma_{22}k_1^2 + \sigma_{11}k_3^2 + \sigma_{22}k_3^2)|\tilde{\eta}|^2c^2 - \\ &c(V_{11}\sigma_{11} + V_{11}\sigma_{22}) - \frac{s_{11}}{2}(\sigma_{11}^2 + \sigma_{22}^2) - s_{12}(\sigma_{11}\sigma_{22}) + \sigma_{11}u_{m1} + \sigma_{22}u_{m2} \end{aligned} \quad (\text{A.18})$$

Where an ‘‘elastic’’ part of Eq.(A.18) could be transformed as follows

$$\begin{aligned} &\sigma_{11}(u_m - V_{11}c - B_{11}k_1^2|\tilde{\eta}|^2c^2 - B_{12}k_3^2|\tilde{\eta}|^2c^2) + \sigma_{22}(u_m - V_{11}c - B_{12}k_1^2|\tilde{\eta}|^2c^2 - \\ &B_{12}k_3^2|\tilde{\eta}|^2c^2) - \frac{s_{11}}{2}(\sigma_{11}^2 + \sigma_{22}^2) - s_{12}(\sigma_{11}\sigma_{22}) = \sigma_{11}(u_m - V_{11}c - B_{11}k_1^2|\tilde{\eta}|^2c^2 - \\ &B_{12}k_3^2|\tilde{\eta}|^2c^2) + \sigma_{22}(u_m - V_{11}c - B_{12}k_1^2|\tilde{\eta}|^2c^2 - B_{12}k_3^2|\tilde{\eta}|^2c^2) - \frac{1}{4}((s_{11} + s_{12})(\sigma_{11} + \\ &\sigma_{22})^2 + (s_{11} - s_{12})(\sigma_{11} - \sigma_{22})^2) = \\ &\frac{(2(u_m - V_{11}c) - (B_{11} + B_{12})k_1^2|\tilde{\eta}|^2c^2 - 2B_{12}k_3^2|\tilde{\eta}|^2c^2)^2}{4(s_{11} + s_{12})} + \frac{((B_{11} - B_{12})k_3^2|\tilde{\eta}|^2c^2)^2}{4(s_{11} - s_{12})} \end{aligned} \quad (\text{A.19})$$

Finally, evident form of the free energy renormalization under misfit stress appearance is

$$\begin{aligned} \Delta\tilde{F}_{FE} &= \left( g - \frac{(u_m - V_{11}c)(B_{11} + B_{12})}{s_{11} + s_{12}} \right) c^2k_1^2|\tilde{\eta}|^2 + \left( g - \frac{2(u_m - V_{11}c)B_{12}}{s_{11} + s_{12}} \right) |\tilde{\eta}|^2c^2k_3^2 + \left( \frac{1}{4} \frac{(B_{11} + B_{12})^2c^4}{s_{11} + s_{12}} + \right. \\ &\left. \frac{1}{4} \frac{(B_{11} - B_{12})^2c^4}{s_{11} - s_{12}} \right) k_1^4|\tilde{\eta}|^4 + \left( \frac{(B_{12})^2c^4}{s_{11} + s_{12}} \right) k_3^4|\tilde{\eta}|^4 + \left( \frac{(B_{11} + B_{12})B_{12}c^4}{s_{11} + s_{12}} \right) k_1^2k_3^2|\tilde{\eta}|^4 \end{aligned} \quad (\text{A.20})$$

## REFERENCES

- 
- [1] J. F. Scott, Data storage: Multiferroic memories, *Nature materials* **6**, 256 (2007).
- [2] M.D. Glinchuk, A.V. Ragulya, V.A. Stephanovich. *Nanoferroics*. Springer Series in Materials Science, 177 (2013) ISBN 978-94-007-5992-3
- [3] P Sharma, P Schoenherr, J Seidel. Functional Ferroic Domain Walls for Nanoelectronics. *Materials* **12**, 2927 (2019)
- [4] J. Valasek, Piezoelectric and allied phenomena in Rochelle salt, *Phys. Rev.* **17**, 475 (1921).
- [5] N. Balke, B. Winchester, W. Ren, Y.-H. Chu, A. N. Morozovska, E. A. Eliseev, M. Huijben, R. K. Vasudevan, P. Maksymovych, J. Britson, S. Jesse, I. Kornev, R. Ramesh, L. Bellaiche, L.-Q. Chen, and S. V. Kalinin. Enhanced electric conductivity at ferroelectric vortex cores in BiFeO<sub>3</sub>. *Nature Physics* **8**, 81 (2012)
- [6] B. Winchester, N. Balke, X. X. Cheng, A. N. Morozovska, S. Kalinin, and L. Q. Chen. Electroelastic fields in artificially created vortex cores in epitaxial BiFeO<sub>3</sub> thin films. *Applied Physics Letters*, **107**, 052903 (2015)
- [7] A. N. Morozovska, E. A. Eliseev and S. V. Kalinin. Topological Defects in Ferroic Materials. Chapter 8 in *Topological Structures in Ferroic Materials*. Springer Series in Mater. Sci. **228**, 181-197 (2016).
- [8] M. J. Han, E. A. Eliseev, A. N. Morozovska, Y. L. Zhu, Y. L. Tang, Y. J. Wang, X. W. Guo, X. L. Ma. Mapping gradient-driven morphological phase transition at the conductive domain walls of strained multiferroic films. *Phys. Rev. B*, **100**, 104109 (2019)
- [9] M. Fiebig, Revival of the magnetoelectric effect, *Journal of Physics D: Applied Physics* **38**, R (2005).
- [10] N. A. Spaldin and M. Fiebig, The renaissance of magnetoelectric multiferroics, *Science* **309**, 391 (2005).
- [11] A. P. Pyatakov and A. K.Zvezdin, Magnetoelectric and multiferroic media, *Physics-Uspexhi* **55**, 557 (2012).
- [12] M. Fiebig, T. Lottermoser, D. Meier, and M. Trassin, The evolution of multiferroics, *Nature Reviews Materials* **1**, 16046 (2016)
- [13] J.M. Rondinelli and N.A. Spaldin, Structure and properties of functional oxide thin films: insights from electronic structure calculations, *Advanced materials* **23**, 3363 (2011).
- [14] A. N. Morozovska, E. A. Eliseev, Y. A. Genenko, I. S. Vorotiahin, M. V. Silibin, Ye Cao, Y. Kim, M. D. Glinchuk, and S. V. Kalinin. Flexocoupling impact on the size effects of piezo- response and conductance in mixed-type ferroelectrics-semiconductors under applied pressure. *Phys. Rev. B* **94**, 174101 (2016)
- [15] J. Seidel. Nanoelectronics based on topological structures. *Nature Materials* **18**, 188 (2019).

- 
- [16] E. Hassanpour, M. C. Weber, A. Bortis, Y. Tokunaga, Y. Taguchi, Y. Tokura, A. Cano, T. Lottermoser, and M. Fiebig. Interconversion of multiferroic domains and domain walls. arXiv preprint arXiv:1908.06876 (2019)
- [17] A. P. Pyatakov, Magnetolectricity goes local: From bulk multiferroic crystals to ferroelectricity localized on magnetic topological textures. *Physica B: Condensed Matter* **542**, 59-62 (2018).
- [18] E. A. Eliseev, A. N. Morozovska, C. T. Nelson, and S. V. Kalinin. Intrinsic structural instabilities of domain walls driven by gradient couplings: meandering anferrodistortive-ferroelectric domain walls in BiFeO<sub>3</sub>. *Phys. Rev.B*, **99**, 014112 (2019)
- [19] A. N. Morozovska, E. A. Eliseev, D. Chen, C. T. Nelson, and S. V. Kalinin. Building Free Energy Functional from Atomically-Resolved Imaging: Atomic Scale Phenomena in La-doped BiFeO<sub>3</sub>. *Phys.Rev. B*, **99**, 195440 (2019)
- [20] E. A. Eliseev, I. S. Vorotiahin, Y. M. Fomichov, M. D. Glinchuk, S. V. Kalinin, Y. A. Genenko, and A. N. Morozovska. Defect driven flexo-chemical coupling in thin ferroelectric films. *Physical Review B*, **97**, 024102 (2018)
- [21] H. Thomann, Stabilization effects in piezoelectric lead titanate zirconate ceramics, *Ferroelectrics* **4**, 141 (1972)
- [22] Y. A. Genenko, J. Glaum, O. Hirsch, H. Kungl, M. J. Hoffmann, and T. Granzow, Aging of poled ferroelectric ceramics due to relaxation of random depolarization fields by space-charge accumulation near grain boundaries, *Phys. Rev. B* **80**, 224109 (2009)
- [23] T. Froemling, H. Hutter, and J. Fleig, Oxide Ion Transport in Donor-Doped Pb(ZrxTi1-x)O3: Near-Surface Diffusion Properties, *J. Am. Ceram. Soc.*, **95** [5], 1692 (2012)
- [24] T. Sluka, A. K. Tagantsev, P. Bednyakov, and N. Setter, Free-electron gas at charged domain walls in insulating BaTiO<sub>3</sub>, *Nat. Comm.* **4**, 1808 (2013)
- [25] I. S. Vorotiahin, A. N. Morozovska, and Y. A. Genenko. Hierarchy of Domain Reconstruction Processes due to Charged Defect Migration in Acceptor Doped Ferroelectrics (<http://arxiv.org/abs/1907.02580>)
- [26] A. Kolpak, I. Grinberg, A. Rappe, Polarization Effects on the Surface Chemistry of PbTiO<sub>3</sub> - Supported Pt Films. *Phys. Rev. Lett.* **98**, 166101 (2007)
- [27] Yi-H. Chiu, K.-D. Chang and Y.-J. Hsu. Plasmon-mediated charge dynamics and photoactivity enhancement for Au-decorated ZnO nanocrystals. *J. Mater. Chem. A*, **6**, 4286 (2018)
- [28] M. J. Highland, T. T. Fister, M.-I. Richard, D. D. Fong, P. H. Fuoss, C. Thompson, J. A. Eastman, S. K. Streiffer, and G. B. Stephenson. Polarization Switching without Domain Formation at the Intrinsic Coercive Field in Ultrathin Ferroelectric PbTiO<sub>3</sub>. *Phys. Rev. Lett.* **105**, (2010) 167601.

- 
- [29] S. M. Yang, A. N. Morozovska, R. Kumar, E. A. Eliseev, Y. Cao, L. Mazet, N. Balke, S. Jesse, R. Vasudevan, C. Dubourdieu, and S. V. Kalinin. Mixed electrochemical-ferroelectric states in nanoscale ferroelectrics. *Nature Physics* **13**, 812 (2017)
- [30] S. V. Kalinin, Y. Kim, D. Fong, and A.N. Morozovska: Surface Screening Mechanisms in Ferroelectric Thin Films and its Effect on Polarization Dynamics and Domain Structures. *Rep. Prog. Phys.* **81**, 036502 (2018)
- [31] R.V.Wang, D.D.Fong, F.Jiang, M.J.Highland, P.H.Fuoss, Carol Tompson, A.M.Kolpak, J.A.Eastman, S.K.Streiffer, A.M.Rappe, and G.B.Stephenson, Reversible chemical switching of a ferroelectric film, *Phys.Rev.Lett.*, **102**, (2009) 047601
- [32] D. D. Fong, A. M. Kolpak, J. A. Eastman, S. K. Streiffer, P. H. Fuoss, G. B. Stephenson, Carol Thompson, D. M. Kim, K. J. Choi, C. B. Eom, I. Grinberg, and A. M. Rappe. Stabilization of Monodomain Polarization in Ultrathin PbTiO<sub>3</sub> Films. *Phys. Rev. Lett.* **96**, (2006) 127601
- [33] M. J.Highland, T. T. Fister, D. D. Fong, P. H. Fuoss, Carol Thompson, J. A. Eastman, S. K. Streiffer, and G. B. Stephenson. Equilibrium polarization of ultrathin PbTiO<sub>3</sub> with surface compensation controlled by oxygen partial pressure. *Physical Review Letters*,**107**, no. 18, (2011) 187602.
- [34] G.B. Stephenson, and M.J. Highland, Equilibrium and stability of polarization in ultrathin ferroelectric films with ionic surface compensation. *Physical Review* **B**, **84** (6), (2011) 064107
- [35] A. N. Morozovska, E. A. Eliseev, N. V. Morozovsky, and S. V. Kalinin Ferroionic states in ferroelectric thin films. *Physical Review* **B** **95**, 195413 (2017) (DOI: 10.1103/PhysRevB.95.195413)
- [36] A. N. Morozovska, E. A. Eliseev, N. V. Morozovsky, and S. V. Kalinin. Piezoresponse of ferroelectric films in ferroionic states: time and voltage dynamics. *Appl. Phys. Lett.* **110**, 182907 (2017)
- [37] A. N. Morozovska, E. A. Eliseev, A. I. Kurchak, N. V. Morozovsky, R. K. Vasudevan, M. V. Strikha and S. V. Kalinin. Effect of surface ionic screening on polarization reversal scenario in ferroelectric thin films: crossover from ferroionic to antiferroionic states. *Physical Review* **B** **96**, 245405 (2017)
- [38] G. Grancini, M.K. Nazeeruddin. Dimensional tailoring of hybrid perovskites for photovoltaics. *Nature Reviews Materials* , **4**, 4 (2019)
- [39] N.A. Pertsev, A.G. Zembilgotov, A. K. Tagantsev. Effect of Mechanical Boundary Conditions on Phase Diagrams of Epitaxial Ferroelectric Thin Films *Phys. Rev. Lett.* **80**, 1988 (1998).
- [40] J. S. Speck, and W. Pompe. "Domain configurations due to multiple misfit relaxation mechanisms in epitaxial ferroelectric thin films. I. Theory." *Journal of applied physics* **76**, 466-476 (1994).
- [41] A.Y. Borisevich, A.N. Morozovska, Young-Min Kim, D. Leonard, M.P.Oxley, M.D. Biegalski, E. A. Eliseev and S.V. Kalinin. Exploring mesoscopic physics of vacancy-ordered systems through atomic scale observations of topological defects. *Phys.Rev.Lett.* **109**, 065702 (2012)
- [42] Xiyong Chen, Jinsong Yu, and Stuart B. Adler. *Chem. Mater.* **2005**, *17*, 4537-4546

---

[43] A. G. Khachaturyan, *Theory of Structural Transformations in Solids* (Wiley, New York, 1983), pp. 511–523.

[44] Note that the ordering could affect isotherm. In other words, if we measure stoichiometry as a function of oxygen partial pressure, is there a inflection point/two phase region where ordering starts.

[45] Daniel A. Freedman, D. Roundy, and T. A. Arias, *Phys. Rev. B* 80, 064108 (2009).

[46] A. P. Levanyuk, S. A. Minyukov, and A. Cano, Universal mechanism of discontinuity of commensurate-incommensurate transitions in three-dimensional solids: Strain dependence of soliton self-energy. *Phys. Rev. B* 66, 014111 (2002).

[47] A.N. Morozovska, E.A. Eliseev, JianJun Wang, G.S. Svechnikov, Y.M. Vysochanskii, V. Gopalan, L.-Q. Chen. Phase diagrams and domain splitting in thin ferroelectric films with incommensurate phases. *Phys. Rev. B.* 81. 195437 (2010).